Journal of the Optical Society of America B
OPTICAL PHYSICS

Void and micro-crack generation in transparent materials with high-energy first-order vector Bessel beam

JUSTAS BALTRUKONIS,[1,2,*] ORESTAS ULČINAS,[1,2] SERGEJ ORLOV,[1] AND VYTAUTAS JUKNA[1]

[1]Coherent Optics Laboratory, Center for Physical Sciences and Technology, Sauletekio 3, Vilnius LT-10257, Lithuania
[2]Workshop of Photonics, Altechna R&D, Mokslininku 6A, Vilnius LT-08412, Lithuania
*Corresponding author: justas.baltrukonis@ftmc.lt

Received 10 April 2020; revised 28 May 2020; accepted 2 June 2020; posted 3 June 2020 (Doc. ID 394820); published 25 June 2020

In this work, we present efficient generation of a high-quality vector Bessel beam using an S-wave plate (radial/azimuth polarization converter) together with an ordinary glass axicon. We examine laser-induced modifications in glass with different pulse durations. We achieve material cracking and observe dominant crack propagation directions caused by the generated beam's intensity asymmetry. By translating the beam, we demonstrate potential application of vector Bessel beams and their transverse polarization components for microprocessing of transparent materials using ultra-short pulses.

https://doi.org/10.1364/JOSAB.394820

1. INTRODUCTION

Glass plays an essential role in today's industry as a unique engineering material for applications in architecture, optics, communications, and various high-technology fields. It is essential for the world's technological development as never before—solar panels, microelectronics, and touch-screens are just a few examples of this vastly growing field. Glass processing capabilities have to keep up with the growing demand, especially for intricate processed glass shapes that will be used in novel technological solutions. Slow and wasteful conventional techniques such as diamond saw dicing, scribe-cleave [1], and water jet [2] are being gradually replaced by more efficient and sustainable lasers utilizing technologies where speed, micrometer-scale quality, and dust-free processes are key factors [3,4].

Various cutting techniques involving laser radiation show great advantages [5,6]; however, industrialization and use of high-peak-power ultra-short pulsed lasers stand out. A minimized thermal effect together with highly nonlinear absorption allows for precise machining process control. Particularly, high laser pulse energy densities are able to induce very localized structural modifications causing stress and micro-crack formation in volumes of bulk material. The cutting process is realized by arranging modification along the desired direction to create a preferential plane of cleaving—so-called stealth-dicing [7]. For high-quality glass cutting applications, a uniform modification along the total thickness of the material is required. The tightly focused Gaussian beams are used to minimize the beam diameter and consequently the material damage area for micro- and nano-fabrication purposes. However, these beams are unable to produce the uniform modification throughout the sample because the thickness of the material exceeds the beam Rayleigh diffraction length; therefore, the material is modified only partly, and translation through the material thickness is used. However, this process increases the processing time and generates nonuniform modification. The salvation comes from the employment of much higher length/width ratio Gaussian–Bessel or modified Gaussian–Bessel beams that increase the productivity and quality of transparent material processing [8].

Bessel beams have gained popularity in laser microprocessing of transparent materials due to beneficial properties: non-diffractive propagation [9], extended focus [10], and easy control of beam size [11], which make them perfect for applications to high aspect ratio micro-void formation [12] and transparent material cutting [13] using induced micro-crack propagation techniques with picosecond [14] or femtosecond [15] laser pulses. Design of the Bessel zone [16–18] further improves properties of nondiffracting beams making them more appealing for laser microprocessing applications [19,20]. It was quickly noticed that the beam profile's asymmetry has the influence to crack propagation direction, and by controlling it, high-quality and ultra-fast glass cutting via cracking can be achieved [21,22]. The use of non-diffracting beams for micro-fabrication purposes is highly investigated, as it enables to enhance the quality or make material processing more efficient [23]. The beam transverse intensity profile shaping is in demand, and generation of a variety of multi-peak and asymmetrical beams is investigated in the literature [24,25]. Many of

these interesting beams have not yet been tested in laser processing or other fields and demand further research to uncover their possible advantages.

In this work, we examine generation and application of transparent material processing of a more exotic alternative—the vector Bessel beam (VBB) ant its transverse polarization components [26]. We generated VBB using a standard glass axicon [27] and an S-wave plate (manufactured by Workshop of Photonics)—a radial/azimuth polarization converter [28]. VBB has a doughnut-shaped symmetrical transverse beam intensity profile, while its orthogonal components feature a highly asymmetrical double-peak intensity profile, i.e., individual peaks with elliptical shape, while a double-peak beam shape elongates the overall transverse beam intensity profile. We generated a high-quality, high-energy VBB, and this proposed setup withstood a 1.5 mJ energy, 158 fs FWHM duration pulses at 1030 nm, which was the limit of our laser. Higher-energy intensity pulses could be used to transform them into a VBB by scaling the optical elements used in the setup. These vector beams could find use in various physics fields, while in this paper, we focus on investigation of modifications induced in fused silica and SCHOTT D263t glass and observe dominant micro-cracking directions as a result of beam intensity asymmetry and employ these beams as a glass-cutting application.

2. THEORETICAL BACKGROUND

A Bessel beam has a spatial amplitude distribution proportional to $J_0(\beta_0 r)$, where J_0 is the zeroth-order Bessel function of the first kind, r is a radial coordinate, and β_0 is a radial frequency [9]. An unperturbed Bessel beam does not diffract in the case of free propagation and is distinguished by an intense central peak surrounded by decreasing intensity rings on the periphery that extend up to infinity. The experimentally realized spatially limited (apertured) Bessel beams may inherit invariable propagation; however, it extends only in a limited length called the Bessel zone [27,29]. The most commonly used method to experimentally generate Bessel beams is with the use of a glass cone called an axicon. This optical element adds a cone-shaped phase profile to the incoming beam, which for the Gaussian beam can be written as

$$E(r, \varphi) = a_0 \exp(-r^2/d^2 - i\beta_0 r), \tag{1}$$

where d is the beam radius, φ is an azimuth, and β_0 is a phase gradient determined by an axicon shape and can be expressed as $\beta_0 \approx 2\pi(n_a - 1)\alpha/\lambda$, where λ is the wavelength, n_a is the refraction index, and α is the wedge angle of the axicon. The maximum beam intensity change with the propagation distance has a distinct form proportional to $z\exp(-z^2)$, which has a steeper ascent than descent.

A Bessel beam can also be visualized as an interference of plane waves whose wave-vectors are placed on a cone; therefore, the spectrum of such a beam is a ring. The apodized Bessel beam with a Gaussian, or in other words experimentally generated, beam will have the ring structure of the spatial spectrum; just the thickness of a ring is proportional to the apodization function. For instance, the spatial spectra of the Bessel–Gauss beam can be expressed as

$$S(\beta, \theta) = \pi d^2 I_0(\beta_0 \beta d^2/2) \exp[-(\beta_0^2 + \beta^2)d^2/4], \tag{2}$$

where I_0 is the modified Bessel function of zeroth order, β is the spectral radius, and θ is the spectral azimuth. For most practical cases [27], $\beta d \gg 1$, and we can use the relation $I_0(x) \approx e^x/\sqrt{2\pi x}$ to obtain

$$S(\beta, \theta) \approx \frac{\exp[-(\beta - \beta_0)^2 d^2/4]d}{\sqrt{\beta_0 \beta/\pi}}. \tag{3}$$

Thus, the spatial spectra of the Bessel–Gauss beam has a Gaussian profile, which is located around the the carrier frequency $\beta_0 = k \sin\alpha_B$, where α_B is the angle of the Bessel beam.

The essence of our paper is the use of an S-wave plate to modify the spatial polarization distribution of a beam incoming to an axicon. The S-wave plate [28] converts a linearly polarized Gaussian beam into radially/azimuthally polarized beams [30]. The converter is encoded in the so-called geometrical phase element [31,32]. The basic operation modus can be described using the formalism of Jones matrices. Let us assume that a nanograting acts as a retarder, which introduces phase delay of kR. An optical element produced using this retardation is described as

$$T(x, y) = R^{-1}[\theta(x, y)]MR[\theta(x, y)]$$

$$= \begin{bmatrix} \cos^2\theta + e^{ikR}\sin^2\theta & (1 - e^{ikR})\cos\theta\sin\theta \\ (1 - e^{ikR})\cos\theta\sin\theta & e^{ikR}\cos^2\theta + \sin^2\theta \end{bmatrix}, \tag{4}$$

where $R(\theta)$ is the rotation matrix, M is the Jones matrix of a retarder, which represents local behavior of the nanogratings, and $\theta(x, y)$ is the local orientation of the nanogratings. For an S-wave plate, we have to choose $kR = pi$; this gives us the following expression:

$$T(x, y) = \begin{bmatrix} \cos 2\theta(x, y) & \sin 2\theta(x, y) \\ \sin 2\theta(x, y) & -\cos 2\theta(x, y) \end{bmatrix}. \tag{5}$$

Next, we have to constitute $\theta(x, y) = \varphi/2$, which results in the expression of the Jones matrix $T(x, y)$ of the S-wave plate. In a rather trivial fashion, we can demonstrate its action on the linearly polarized light:

$$E_{\text{rad}}(x, y) = \begin{bmatrix} \cos\varphi & \sin\varphi \\ \sin\varphi & -\cos\varphi \end{bmatrix} \begin{bmatrix} 1 \\ 0 \end{bmatrix},$$

$$E_{\text{azi}}(x, y) = \begin{bmatrix} \cos\varphi & \sin\varphi \\ \sin\varphi & -\cos\varphi \end{bmatrix} \begin{bmatrix} 0 \\ 1 \end{bmatrix}. \tag{6}$$

Thus, an S-wave plate produces radially and azimuthally polarized beams, depending on the input polarization state of the beam. When the linearly polarized Gaussian beam propagates through the S-wave plate, the axicon [multiply (6) with (1)] will generate a first-order VBB that will be used in our experiments to generate cracks in transparent materials. The S-wave plate can be placed at the spectrum [multiply (6) with (2)], which, again due to cylindrical symmetry, will generate VBB; however, in this configuration, the spectral and polarization filtering is complicated and was not used in the experiments.

3. EXPERIMENTAL SETUP

Generation of first-order VBB and glass modification experiments were performed using an ultra-fast PHAROS (Light Conversion) Yb:KGW laser (transform limited pulse duration of 158 fs FWHM, up to 1.5 mJ pulse energy with carrier wavelength of 1030 nm) together with an axicon-based (wedge angle $\alpha = 1°$) VBB generation system featuring an S-wave plate in the beam path as a polarization converter. The simplified experimental setup is depicted in Fig. 1. A polarizer that could be rotated transversely was placed after the S-wave plate and used to separate the beam's orthogonal polarization components. The proposed approach is able to generate VBB with high energy and quality because the S-wave plate has a high damage threshold of 63,4 J/cm^2 at 1064 nm in the nanosecond regime (10 ns) and 2,2 J/cm^2 at 1030 nm in the femtosecond regime (212 fs) [33].

The generated beam was imaged using a 4f demagnifying setup ($M = 31.25$) creating a $\alpha_B \sim 14.06°$ Bessel cone angle in air. A CCD camera was used to measure transverse and longitudinal intensity distributions. We encountered a drawback due the use of a glass axicon to generate Bessel beams. The high axial intensity modulation appears due to the non-ideal rounded tip of an axicon [12,21]. Such an imperfect axicon not only bends light at its designed single conical angle but generates a broad angular spectrum causing unwanted axial intensity modulation via interference. The same imperfection also alters a central core radius that results in generation of distorted VBBs and hence may leave footprints by generating an irregular modification channel. A proposed method to reduce this effect is the use of a spatial filter at the focal plane of the first lens of a 4f imaging system [12], which blocks undesirable spatial frequencies. A custom spatial filter was made by selectively ablating a ring (4 mm in diameter, width 0.17 mm) off a chrome layer on a glass substrate. This filter blocks both higher and lower frequency spatial components, allowing elimination of most of the unwanted irregularities and generation of a beam similar to theoretically calculated (3) VBBs (Figs. 2 and 3).

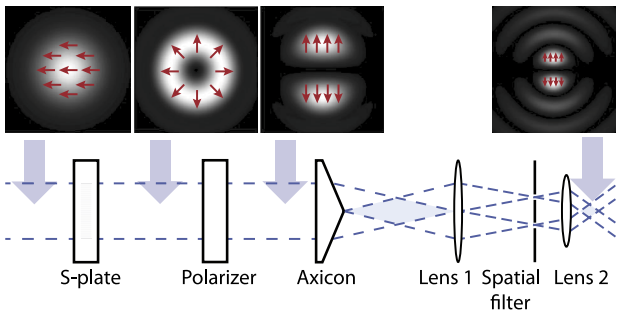

Fig. 1. Simplified experimental setup for single transverse intensity component of radially polarized vector Bessel beam generation. Red arrows indicate polarization vectors. Lens 1 and lens 2 represent the 4f demagnifying imaging system. Azimuthally polarized vector Bessel beams can be generated by rotating polarization of incoming beam by 90° before the setup or by rotating the S-wave plate.

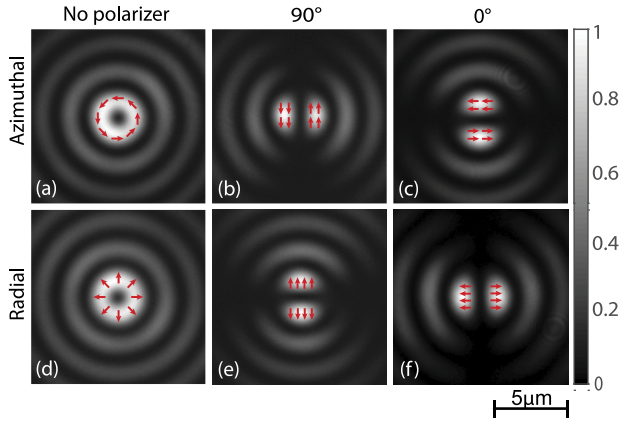

Fig. 2. Measured beam transverse fluence profiles of experimentally generated azimuthally (a) and radially (d) polarized vector Bessel beams and their single polarization components at different polarizer rotation angles (b), (c), (e), (f). Red arrows indicate polarization vectors.

4. RESULTS

A. Generated Beam

The ability to rotate incoming beam polarization by 90° allowed us to generate and investigate both azimuthally and radially polarized VBBs. In both cases, a symmetrical, doughnut-shaped transverse beam profile was registered with minor intensity variations over the ring circumference. A polarizer axis positioned 0° and 90° with respect to the table plane was used to separate orthogonal polarization components. Beam transverse intensity distribution featuring a double-peak pattern was observed in all cases. They differed only in the position of the peaks because the same polarization vector components for the radially and azimuthally polarized beams are found at orthogonal positions with respect to the beam center as expected from (6). The red arrows in Fig. 2 represent polarization vectors for all cases. Due to the fact that the polarization vector angle changes linearly with respect to the azimuth angle, the direction of double-peak orientation may be controlled just by rotating the polarizer.

Longitudinal intensity profiles were measured by scanning the beam with an objective and CCD camera in the z direction. The measured intensity profile of the radially polarized beam in the xz plane (Fig. 3) shows no major distortions or intensity modulation along the z axis and maintains a quality transverse intensity profile through all the propagation length. The same good quality of propagation was registered with azimuthally

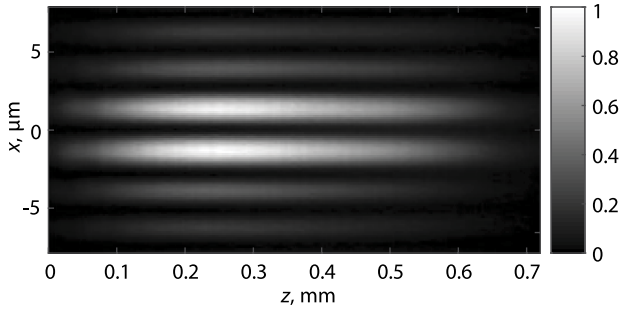

Fig. 3. Measured beam intensity profile in the xz plane of the experimentally generated radially polarized vector Bessel beam.

polarized beams and their separate components. Beam length in propagation direction z was evaluated to be 0.375 mm FWHM in air with a constant ring radius of 1.3 μm (measured from beam center to ring peak intensity).

B. Modifications in Glass

The generated high-quality VBBs and their filtered transverse polarization component beams were employed to induce single-shot material modifications inside glass samples. Laser pulse duration was varied to observe different types of generated material modifications. The transform limited pulse having a duration of 158 fs was chirped to increase pulse duration up to 5 ps by detuning the laser's compressor.

The thick UV-grade fused silica (UVFS) sample used in experiments was a rectangular cuboid with dimensions of 5 mm × 5 mm × 20 mm that allowed us to fit all the length of the VBB. The four polished surfaces allowed to transport the VBB inside the sample and later observe the induced volume modifications with a microscope from the transverse surface. The volume modifications in UVFS were induced by 137.5 μJ energy pulses measured just after the last focusing lens. The introduction of a polarizer removes half of the energy, leaving total energy of 67.25 μJ for single polarization component pulses. Despite lower pulse energy, local glass modification is expected to be similar because the maximum energy density remains almost the same compared to polarization unfiltered beams. UVFS volume modifications produced by the radial polarization beam of single polarization having 67.25 μJ energy and variable pulse duration were registered with a microscope objective having magnification of ×50 and NA of 0.75. We visually observed generation of two parallel voids only when the pulse duration was increased more than 2 ps FWHM. Shorter pulses were unable to generate observable voids. They produced only a localized slight refractive index change that was hard to notice; therefore, they are not presented in the figure. The visible voids were generated with pulses longer than 2 ps, and best results were observed for a pulse duration of 5 ps. The measured distances between the parallel voids were 2.68 μm with each having a diameter less than 1 μm (see Fig. 4). Longer pulses generated more pronounced voids; however, their lengths were shorter and therefore less uniform.

There is a large debate on the subject of the best energy deposition tactics while using Bessel beams that is reflected by many publications on this subject [12,34–39]. In short, the energy deposition process is highly influenced by plasma generation processes, nonlinear propagation of the pulse, and plasma recombination rate, while the material modification can also be affected by temperature diffusion, phase transformation, beam-induced stress cracking, pressure waves generation, and others, which makes the subject a complex mix of many nonlinear material responses. Having established that pulse duration of 5 ps showed generation of the best voids in UVFS, we proceeded to analyze the void formation with full VBB and compare it to the results achieved with its transverse polarization components. The microscope images (Fig. 5) taken in a perpendicular direction to the incident laser beam reveal that double-line voids are maintained along the full modified length and closely match measured intensity profiles. Volume modification induced with full VBB indicates generation of a tube void, but it does not sustain ideal symmetry [see Fig. 5(c)]. The observed stronger modified material zones could be due to slight intensity modulation of the transverse intensity profile that would suggest the material modification strength is sensitive to beam intensity distribution. We registered a whole beam intensity profile and analyzed intensity irregularities over the azimuth angle of the first ring. A bump of intensity measuring 15% was observed due to a nonperfect S-wave plate and/or optical setup, and because the location of the intensity bump coincides with the stronger volume modification position, it suggest that the higher-quality beam could in principle increase the quality of a void tube.

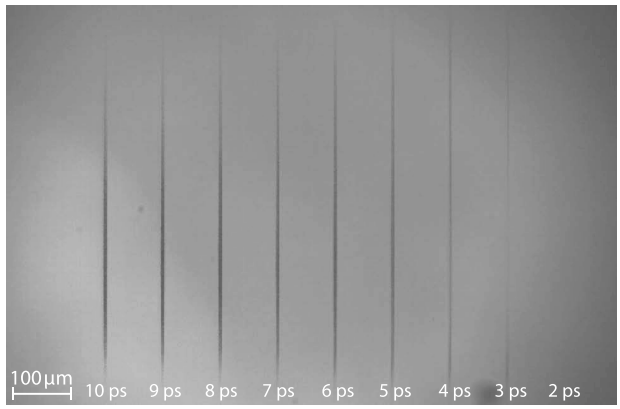

Fig. 4. Transmission microscopy images of the change in the UVFS sample volume modification with respect to pulse duration generated by single polarization of radially polarized VBB. The pulse energy was fixed to 67.25 μJ, and pulse duration varied from 2 ps to 10 ps FWHM.

To investigate applicability of such beams for glass-cutting applications, we analyzed induced material cracking with the VBB. A thin, 300 μm thick sheet of widely commercially used D263T glass was employed. This glass features a high thermal expansion coefficient of $a = 7.2 \times 10^{-6}\mathrm{K}^{-1}$ compared with fused silica having $a = 0.55 \times 10^{-6}\mathrm{K}^{-1}$, thus enhancing the effect of extended micro-crack formation. Beams were separated 100 μm apart to minimize or eliminate effects of extraneous stress caused by adjacent modifications, and higher pulse energies were used to enhance stress and crack formation. Both azimuthally and radially polarized VBBs were investigated. Modifications were examined using a 100× 0.9 NA microscope objective in a reflection configuration for surface images and transmission configuration for imaging glass volume. In the case of the doughnut-shaped beam, we observed that both polarization states showed similar material modification results: symmetrical, doughnut-shaped entry and exit surface modifications followed by irregular volume cracking [see Figs. 6(a), 6(d), 6(g), and 6(j)]. The cracks that formed did not have dominant directions and could be only slightly influenced by transverse intensity irregularities, partly reflected in slightly distorted volume modification in Fig. 5(c). We also did not observe damage tracks or cracking dependence on the polarization state of VBB at the used micro-fabrication parameters.

On the other hand, the single polarization component of VBB has highly expressed asymmetrical transverse intensity distribution, and in this case, the generated cracks did

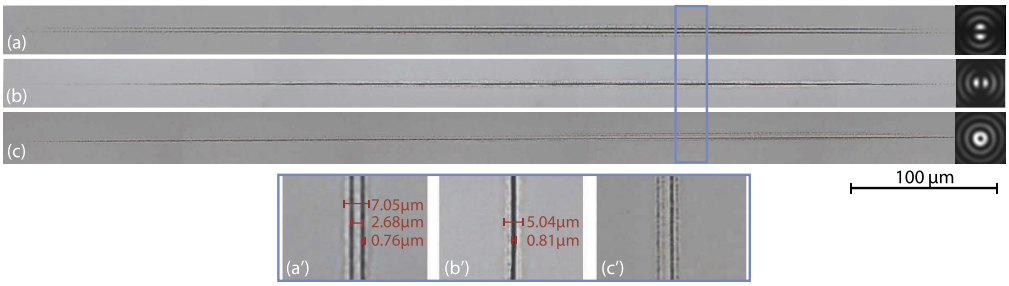

Fig. 5. Transmission microscopy images of modifications in fused silica sample with (c) radially polarized vector Bessel beam (pulse energy 137.5 µJ) and (a), (b) its orthogonal polarization components (67.25 µJ). Pulse duration 5 ps. Images (a')–(c') in the blue rectangle indicate enlarged sections. Beam profiles on the right illustrate beam orientation and intensity distribution in each case.

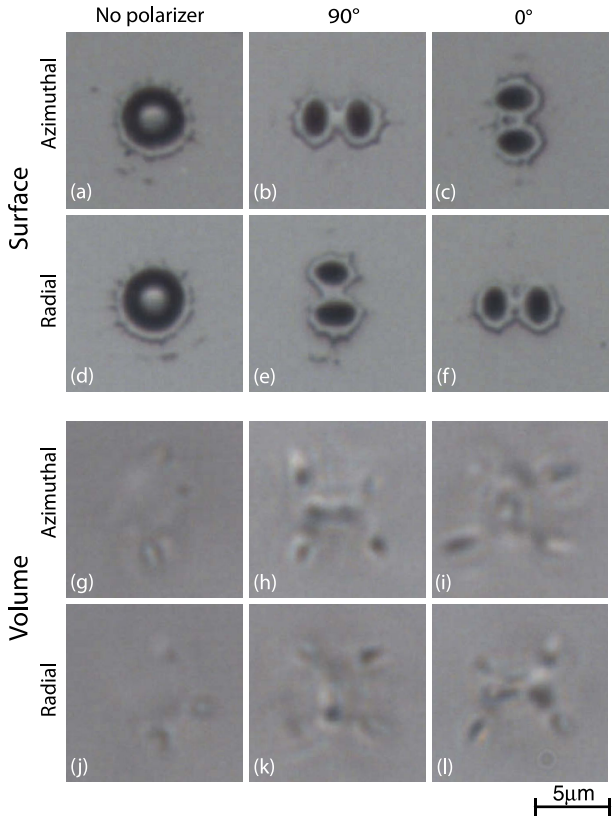

Fig. 6. Microscope images of voids formed on SCHOTT D263T glass surface (top images, reflection microscopy) and visible cracks in volume (bottom images, transmission microscopy) with (a), (g) radially and (d), (j) azimuthally polarized VBB (pulse energy 232.3 µJ) and (b), (c), (e), (f), (h), (i), (k), (l) its orthogonal polarization components (pulse energy 114.1 µJ). Pulse duration 5 ps.

show dependence on the direction of the two intensity peaks [Figs. 6(b), 6(c), 6(e), and 6(f)]. First, we observe the generated damage profiles on the glass surface that extends all the way to the back of the glass plate and consists of two voids. The individual void is elliptically shaped with the longer and shorter axes having dimensions of 2.06 µm and 1.24 µm, respectively, resulting in a ratio of 1.66 µm. The separation between the center of the voids is 2.58 µm, and the ratio between the furthermost void edges and individual void's longer ellipse axis is calculated to be 1.85. Analysis of the intensity profiles (Fig. 2) gives ratios of 1.63 and 1.84, respectively, at half maximum intensity, which proves a good method to estimate the damage ellipticity. Therefore, the damage of the material has two elongation directions: the individual void elongation and the overall elongation of double-void modification, which are perpendicular to each other. Microscope images taken from the volume [Figs. 6(h), 6(i), 6(k), and 6(l)] of the sample indicate clear dominant cracking directions. The cracking direction follows the individual void's longer ellipse axis direction having a 20° angle of deflection that was probably caused by simultaneous generation of two voids and therefore generation of secondary ellipticity of the damage. Such behavior indicates that ellipticity of a single intensity peak dominates the overall asymmetry in multi-peak beam configuration and is the key factor for crack direction predictions. The glass cracking direction rotates with the rotation of the peaks; therefore, the cracking direction depends on transverse intensity distribution. No significant cracking or void formation dependence on polarization direction was observed at the used fabrication parameters.

Cutting of the transparent materials is accomplished by creating adjacent modifications thorough full sample thickness placed in line placed close to each other creating a joining crack. If the material is not prone to cracking, the double-peaked beam will increase the quality of cutting just by correctly orientating the double-peak structure in the direction of cutting.

However, for materials prone to cracking, one has to take into account that non-axial cracking is produced by these particular beams. We analyzed the ability to use cracking to our advantage while cutting the SCHOTT D263T glass with VBB beams. We noticed that a full VBB does not have a tendency to create directional cracks; however, the single polarization component of the VBB does. We were able to find the micro-fabrication parameters where the cracks connect in the direction of the beam translation for both cases—first, when the direction of the two intensity peaks (overall beam asymmetry) coincides, and second, when it is perpendicular to the direction of translation.

Figure 7 shows in-depth analysis of joint crack formation and the effect on cleaved surface roughness in cases when the direction of the two intensity peaks coincides with the direction of movement (left) and when directions are perpendicular to each other (right). Figures 7(a) and 7(b) show cracking line formation in volume, while Figs. 7(c) and 7(d) are on the surface of the sample. When both directions coincide the adjacent beams and therefore modifications were placed 11 µm between the beam

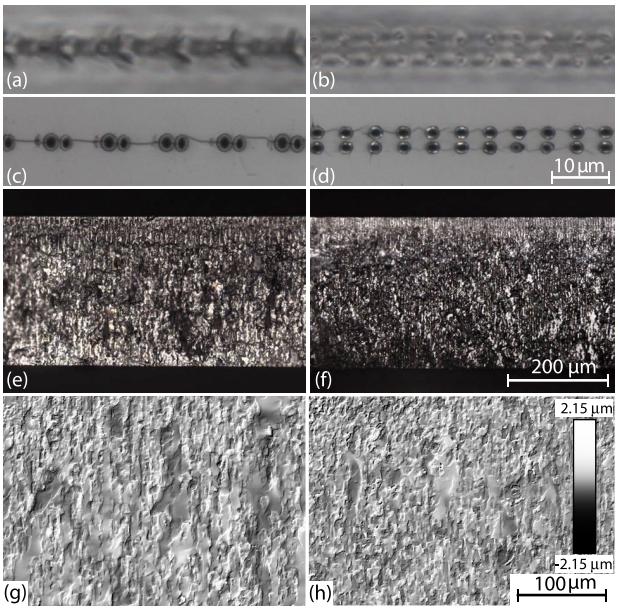

Fig. 7. Transmission microscopy images of joined cracks in volume (a), (b), reflection microscopy images of surface (c), (d), from side (e), (f), and surface topography images (g), (h) of SCHOTT D263t glass sample with radially polarized vector Bessel beam component, when the direction of the two intensity peaks coincides (left) and is perpendicular (right) to the direction of beam movement [pulse energy 291.6 μJ (a) and 175.1 μJ (b)]. Pulse duration 5 ps.

centers and distinct crack joined the voids. All experiments were done with pulses of 5 ps duration. We observed that the laser pulse energy needed to join the cracks was higher than the energy needed to produce only voids extending through the whole sample thickness; in this particular case, when the beams were 11 μm apart, we used pulses with 291.6 μJ of energy. Even though the image of the surface indicates a single crack line, the volume image reveals additional perpendicular cracks created at every modification due to single void elongation, as illustrated in Fig. 6.

In the case when the direction of the double peak is perpendicular to the beam translation (Fig. 7, right) the cracks formed by a single beam have almost the same direction as the fabricated cleaving plane; therefore, it is expected for the material to be able to connect them more easily. Two perpendicular joint crack lines were obtained and are visible in the volume and on the surface with no perpendicular cracking. The cleanest and repeated crack merger was achieved when the separation between the beams was 5 μm and pulse energy was set to 175.1 μJ. Significantly lower pulse energies were needed than in the previous case to create a crack line, indicating that the correct beam orientation plays an essential role.

The quality of the cuts was tested by breaking the sample at the generated cleaving plane and observing the transverse plane under the microscope and measuring its surface topography with a confocal profilometer (Sensofar S neox) [see Figs. 7(e), 7(f) and 7(g), 7(h)]. Although in both cases, we were able to cleave the sample, the configuration depicted on the left side of the figure shows greater surface roughness of the cleavage surface, while on the right side, the surface is smoother. The retrieved surface quality values are $S_q = 0.5423$ μm and 0.7164 μm, and $S_p = 2.8427$ μm and 4.1718 μm for surfaces shown in Figs. 7(e) and 7(f), respectively. The measurements were done according to ISO 25178 standard, where S_q is the root mean square height—the rms height of all data points from the mean surface height (rms roughness)—and S_p is maximum peak height—the difference between the mean surface height and the highest point within data. It is also visible that the cleavage surface for the leftside case was smooth with good surface quality only at the front face of the sample indicating, a straight crack connection; however, they do not stay regular deeper in the glass volume. We observe a crack direction change, and as a result, the surface obtains irregularly shaped material leftovers where the crack is not fully parallel to the cleaving plane. This effect was anticipated, as we observed that the crack (stress vector) direction induced by single pulse modification did not coincide with the direction of beam translation, while in the rightside case (Fig. 7), the crack direction generated by a single peak was very close to the direction of translation and estimated to be only 20° off the straight translation trajectory. The cracks tend to connect over the full length of the glass sample showing a bit smoother surface through the full depth of the sample. Yet, the drawback of this configuration is that double crack lines are formed, and one of the cleaved sample pieces has a leftover crack line on the edge. Therefore, the cracks formed by all consecutive beams tend to weaken the material in the preferable direction throughout the full depth.

5. CONCLUSION

A method for generation of a high-quality, high-energy VBB using an axicon and S-wave plate was proposed and successfully implemented. High-quality radially and azimuthally polarized VBBs and individual orthogonal polarization components were generated and tested for micro-fabrication applications of transparent media. It was shown that VBB generates high aspect ratio voids, and in principle, the long tube shape voids are possible to fabricate. The glass cracking ability of these beams was investigated, and results show that there are no clear dominant micro-cracking directions when VBB is used. However, a single polarization component generates cracks stretching along the direction of an individual elliptical void's longer ellipse axis with a small 20° deflection. The applicability of such beams for glass cutting with micro-crack formation was also shown and investigated. Two cases of cutting the glass were investigated. First, the direction of the two intensity peaks coincides with the direction of beam translation, and second, the directions are perpendicular. A smoother cleavage surface was obtained and lower pulse energies were needed for the second case because the induced material stress caused by the asymmetrical incident beam and stress caused by nearby modifications had almost the same direction, easing the crack joining between adjacent modifications. Such observations lead to the conclusion that the ellipticity of a single intensity peak dominates the overall asymmetry in multi-peak beam configuration and is the key factor for laser-induced cracking direction.

Funding. Lietuvos Mokslo Taryba; European Social Fund (09.3.3-LMT-K-712-01-0167).

Acknowledgment. This project has received funding from the European Social Fund (project No 09.3.3-LMT-K-712-01-0167) under grant agreement with the Research Council of Lithuania (LMTLT).

Disclosures. The authors declare no conflicts of interest.

REFERENCES

1. C. Pan, C. Hsieh, C. Su, and Z. Liu, "Study of cutting quality for TFT-LCD glass substrate," Int. J. Adv. Manuf. Technol. **39**, 1071–1079 (2008).
2. U. Aich, S. Banerjee, A. Bandyopadhyay, and P. K. Das, "Abrasive water jet cutting of borosilicate glass," Procedia Mater. Sci. **6**, 775–785 (2014).
3. H. Misawa and S. Juodkazis, *3D Laser Microfabrication: Principles and Applications* (Wiley, 2006).
4. R. Osellame, G. Cerullo, and R. Ramponi, *Femtosecond Laser Micromachining: Photonic and Microfluidic Devices in Transparent Materials* (Springer, 2012), Vol. **123**.
5. S. Nisar, L. Li, and M. Sheikh, "Laser glass cutting techniques—a review," J. Laser Appl. **25**, 042010 (2013).
6. S. Butkus, D. Paipulas, Ž. Viburys, A. Alesenkov, E. Gaižauskas, D. Kaškelytė, M. Barkauskas, and V. Sirutkaitis, "Rapid microfabrication of transparent materials using a filamented beam of the IR femtosecond laser," Proc. SPIE **8972**, 897216 (2014).
7. W. H. Teh, D. S. Boning, and R. E. Welsch, "Multistrata subsurface laser-modified microstructure with backgrind-assisted controlled fracture for defect-free ultrathin die fabrication," IEEE Trans. Compon. Packag. Technol. **5**, 1006–1018 (2015).
8. M. Duocastella and C. B. Arnold, "Bessel and annular beams for materials processing," Laser Photon. Rev. **6**, 607–621 (2012).
9. J. Durnin, "Exact solutions for nondiffracting beams. I. The scalar theory," J. Opt. Soc. Am. A **4**, 651–654 (1987).
10. M. Zhu, Q. Cao, and H. Gao, "Creation of a 50,000λ long needle-like field with 0.36λ width," J. Opt. Soc. Am. A **31**, 500–504 (2014).
11. M. K. Bhuyan, F. Courvoisier, P.-A. Lacourt, M. Jacquot, L. Furfaro, M. Withford, and J. Dudley, "High aspect ratio taper-free microchannel fabrication using femtosecond Bessel beams," Opt. Express **18**, 566–574 (2010).
12. M. K. Bhuyan, P. K. Velpula, M. Somayaji, J.-P. Colombier, and R. Stoian, "3D nano-fabrication using controlled Bessel-glass interaction in ultra-fast modes," J. Laser Micro Nanoeng. **12**, 274–280 (2017).
13. R. Stoian, M. K. Bhuyan, G. Zhang, G. Cheng, R. Meyer, and F. Courvoisier, "Ultrafast Bessel beams: advanced tools for laser materials processing," Adv. Opt. Technol. **7**, 165–174 (2018).
14. M. Bhuyan, O. Jedrkiewicz, V. Sabonis, M. Mikutis, S. Recchia, A. Aprea, M. Bollani, and P. Di Trapani, "High-speed laser-assisted cutting of strong transparent materials using picosecond Bessel beams," Appl. Phys. A **120**, 443–446 (2015).
15. K. Mishchik, R. Beuton, O. D. Caulier, S. Skupin, B. Chimier, G. Duchateau, B. Chassagne, R. Kling, C. Hönninger, E. Mottay, and J. Lopez, "Improved laser glass cutting by spatio-temporal control of energy deposition using bursts of femtosecond pulses," Opt. Express **25**, 33271–33282 (2017).
16. T. Čižmár and K. Dholakia, "Tunable Bessel light modes: engineering the axial propagation," Opt. Express **17**, 15558–15570 (2009).
17. S. Orlov, A. Juršėnas, and E. Nacius, "Optical Bessel-like beams with engineered axial phase and intensity distribution," J. Laser Micro Nanoeng. **13**, 244–248 (2018).
18. S. Orlov, A. Juršėnas, J. Baltrukonis, and V. Jukna, "Controllable spatial array of Bessel-like beams with independent axial intensity distributions for laser microprocessing," J. Laser Micro Nanoeng. **13**, 324–329 (2018).
19. F. He, J. Yu, Y. Tan, W. Chu, C. Zhou, Y. Cheng, and K. Sugioka, "Tailoring femtosecond 1.5-μm Bessel beams for manufacturing high-aspect-ratio through-silicon vias," Sci. Rep. **7**, 40785 (2017).
20. R. Li, X. Yu, T. Peng, Y. Yang, B. Yao, C. Zhang, and T. Ye, "Shaping the on-axis intensity profile of generalized Bessel beams by iterative optimization methods," J. Opt. **20**, 085603 (2018).
21. J. Dudutis, P. Gečys, and G. Račiukaitis, "Non-ideal axicon-generated Bessel beam application for intra-volume glass modification," Opt. Express **24**, 28433–28443 (2016).
22. R. Meyer, M. Jacquot, R. Giust, J. Safioui, L. Rapp, L. Furfaro, P.-A. Lacourt, J. M. Dudley, and F. Courvoisier, "Single-shot ultrafast laser processing of high-aspect-ratio nanochannels using elliptical Bessel beams," Opt. Lett. **42**, 4307–4310 (2017).
23. R. Stoian, M. K. Bhuyan, A. Rudenko, J.-P. Colombier, and G. Cheng, "High-resolution material structuring using ultrafast laser non-diffractive beams," Adv. Phys. X **4**, 1659180 (2019).
24. C. Alpmann, R. Bowman, M. Woerdemann, M. Padgett, and C. Denz, "Mathieu beams as versatile light moulds for 3D micro particle assemblies," Opt. Express **18**, 26084–26091 (2010).
25. S. Orlov, V. Vosylius, P. Gotovski, A. Grabusovas, J. Baltrukonis, and T. Gertus, "Vector beams with parabolic and elliptic cross-sections for laser material processing applications," J. Laser Micro Nanoeng. **13**, 280–286 (2018).
26. A. Dudley, Y. Li, T. Mhlanga, M. Escuti, and A. Forbes, "Generating and measuring nondiffracting vector Bessel beams," Opt. Lett. **38**, 3429–3432 (2013).
27. V. Jarutis, R. Paškauskas, and A. Stabinis, "Focusing of Laguerre-Gaussian beams by axicon," Opt. Commun. **184**, 105–112 (2000).
28. M. Beresna, M. Gecevičius, P. G. Kazansky, and T. Gertus, "Radially polarized optical vortex converter created by femtosecond laser nanostructuring of glass," Appl. Phys. Lett. **98**, 201101 (2011).
29. F. Gori, G. Guattari, and C. Padovani, "Bessel-Gauss beams," Opt. Commun. **64**, 491–495 (1987).
30. T. Bauer, S. Orlov, U. Peschel, P. Banzer, and G. Leuchs, "Nanointerferometric amplitude and phase reconstruction of tightly focused vector beams," Nat. Photonics **8**, 23–27 (2014).
31. F. S. Roux, "Geometric phase lens," J. Opt. Soc. Am. A **23**, 476–482 (2006).
32. P. Gotovski, P. Šlevas, E. Nacius, V. Jukna, S. Orlov, J. Baltrukonis, O. Ulčinas, and T. Gertus, "Formation of optical needles by Pancharatnam-Berry phase element for laser-induced modifications in transparent materials," Proc. SPIE **11268**, 112681Y (2020).
33. "Laser-induced damage threshold (LIDT) measurement report," 2020, https://www.wophotonics.com/wp-content/uploads/2020/03/LIDT-result-fs-regime.pdf.
34. M. Bhuyan, P. K. Velpula, J.-P. Colombier, T. Olivier, N. Faure, and R. Stoian, "Single-shot high aspect ratio bulk nanostructuring of fused silica using chirp-controlled ultrafast laser Bessel beams," Appl. Phys. Lett. **104**, 021107 (2014).
35. P. Polesana, M. Franco, A. Couairon, D. Faccio, and P. Di Trapani, "Filamentation in Kerr media from pulsed Bessel beams," Phys. Rev. A **77**, 043814 (2008).
36. M. A. Porras, A. Parola, D. Faccio, A. Dubietis, and P. Di Trapani, "Nonlinear unbalanced Bessel beams: stationary conical waves supported by nonlinear losses," Phys. Rev. Lett. **93**, 153902 (2004).
37. M. Lamperti, V. Jukna, O. Jedrkiewicz, P. Di Trapani, R. Stoian, T. E. Itina, C. Xie, F. Courvoisier, and A. Couairon, "Invited article: filamentary deposition of laser energy in glasses with Bessel beams," APL Photon. **3**, 120805 (2018).
38. V. Garzillo, V. Jukna, A. Couairon, R. Grigutis, P. Di Trapani, and O. Jedrkiewicz, "Optimization of laser energy deposition for single-shot high aspect-ratio microstructuring of thick BK7 glass," J. Appl. Phys. **120**, 013102 (2016).
39. P. Polesana, A. Dubietis, M. A. Porras, E. Kučinskas, D. Faccio, A. Couairon, and P. Di Trapani, "Near-field dynamics of ultrashort pulsed Bessel beams in media with Kerr nonlinearity," Phys. Rev. E **73**, 056612 (2006).